Electron-phonon coupling and superconductivity in arsenic under pressure

Kevin T. Chan,* Brad D. Malone, and Marvin L. Cohen
Department of Physics, University of California, Berkeley, California 94720, USA and
Materials Sciences Division, Lawrence Berkeley National Laboratory, Berkeley, California 94720, USA
(Received 13 August 2012; revised manuscript received 24 August 2012; published 14 September 2012)

We perform first-principles calculations of the electronic structure, phonon dispersion, and electron-phonon coupling in elemental As at various pressures above and below the rhombohedral $A7$ to simple cubic (sc) structural transition. We find that the electron-phonon coupling constant λ, and hence the superconducting transition temperature T_c, is largest near the structural transition and decreases away from it. Changes in λ as a function of pressure are primarily explained by changes in the density of states at the Fermi level for pressures below the transition, and by changes in phonon frequency for pressures above the transition. Although the couplings to the Γ_1 optical phonon mode (for $A7$) and the R phonon mode (for sc) are large, the contribution of these modes to λ for their respective structures is modest.

DOI: 10.1103/PhysRevB.86.094515 PACS number(s): 74.62.Fj, 74.70.Ad, 74.25.Kc, 74.20.Pq

I. INTRODUCTION

For many materials, applying pressure is known to cause structural phase transitions and changes in superconducting transition temperature (T_c).[1] A striking example is elemental Li, which undergoes several structural phase transitions with increasing pressure and reaches a T_c as high as 20 K.[2–4] Crystalline elemental As is known experimentally to undergo a transition from the rhombohedral $A7$ structure at ambient pressure to the simple cubic (sc) structure at around 25–32 GPa as pressure is increased.[5,6] The stability of the $A7$ structure at ambient pressure and the transition to sc with increasing pressure can be explained by a Peierls distortion mechanism. In such a mechanism, strong coupling of electrons to the sc R and $A7$ Γ_1 optical phonon modes, Fermi surface nesting, a Kohn anomaly are all involved.[7–11]

In addition, As under pressure is superconducting,[12,13] with the most recent study measuring a peak in T_c around the pressure of the phase transition.[14] In this study, this peak in T_c was explained qualitatively by changes in the electronic density of states at the Fermi level (ϵ_F) and the phonon frequencies of the $A7$ Γ_1 optical mode and the sc R mode.

While these phenomena demonstrate that electron-phonon (e-p) coupling is important in As, it would be interesting to understand the role of e-p coupling in more detail. In particular, a precise understanding of the relative importance of changes in the density of states at ϵ_F [$N(\epsilon_F)$], phonon frequency, and e-p matrix elements to changes in T_c would be useful. In addition, the importance of particular phonon wavevectors in superconductivity has been demonstrated in Li and other materials.[15–17] Given that the sc R mode has particular importance in the structural transition in As, its role in superconductivity would also be interesting to understand. Such physical insight might also be applicable to our understanding of other materials that undergo changes in structure and T_c with pressure, such as the other Group V elements.

Detailed studies of e-p coupling are now possible with recent methodological developments and increasing computational power. In particular, a recently developed method based on Wannier functions allows the study of e-p coupling on fine grids in the Brillouin zone (BZ) for electron and phonon states.[18,19]

In the present study, we perform first-principles calculations of the electronic structure, phonon dispersion, and e-p coupling in As as a function of pressure around the $A7$ to sc transition. Our results for T_c are in good agreement with experiment. We verify that the peak in T_c is directly related to the structural transition, and we study the changes as a function of pressure of the phonons, $N(\epsilon_F)$, e-p matrix elements, the e-p coupling constant λ, and T_c. We find that the softening of the $A7$ optical mode/sc R mode does not have a large direct effect on T_c. The main importance of this mode is its role in the $A7$ to sc structural transition, which leads to a large change in $N(\epsilon_F)$ and thus a large change in T_c. Furthermore, we find that the change in T_c above the structural transition pressure is primarily due to changes in average phonon frequency across all modes.

In Sec. II, we briefly describe the $A7$ structure and its relation to the sc structure. The method and computational details for the present study are given in Sec. III. In Sec. IV we present our results, divided into the following subsections: the structure of As as a function of pressure (Sec. IV A) and the e-p properties of the sc structure (Sec. IV B) and the $A7$ structure (Sec. IV C). General trends for e-p coupling as a function of pressure and a comparison of our results to experiment are presented in Sec. V. In Sec. VI we conclude the paper.

II. *A7* AND *sc* STRUCTURES IN ARSENIC

The rhombohedral $A7$ structure contains two atoms per unit cell and can be specified by three parameters: the lattice constant a_{rhom}, the rhombohedral angle α between two direct lattice vectors, and the internal parameter u, which determines the distance between the two atoms in the cell. An $A7$ structure having the same species for its two basis atoms and with $\alpha = 60^\circ$ and $u = 0.25$ is equivalent to the sc structure.[20]

Elemental As at ambient pressure exists in the $A7$ structure with experimentally measured lattice parameters of $a_{\text{rhom}} = 4.1018$ Å, $\alpha = 54.554^\circ$, and $u = 0.2276$ (at 4.2 K).[21] The structure is layered, with each As atom forming strong p-like bonds to each of its three nearest intralayer neighbors, while interlayer bonding is weaker. The stability of the $A7$ structure with respect to sc at ambient pressure can be understood in terms of a Peierls mechanism. The rhombohedral

distortion and the displacement of atoms away from the *sc* positions, as indicated by the decreased u parameter, allow the formation of covalent p-like bonds, open a gap at ϵ_F, and lower the overall energy of the crystal.

As pressure is increased, the energy gain from the Peierls-like distortion with respect to the *sc* structure decreases, and the degree of distortion decreases until the *sc* structure becomes stable at the transition pressure. The transition from $A7$ to *sc* with increasing pressure has been observed experimentally[5,6] and has been the subject of many theoretical studies.[8–11,14,22–29]

The displacement of atoms involved in the transition between the $A7$ and *sc* structures corresponds to the $A7$ Γ_1 optical mode. In the *sc* structure, the wavevector of this mode is at the R point in the BZ.

III. METHOD AND COMPUTATIONAL DETAILS

Our general procedure is as follows. We first determine the structural parameters of As as a function of pressure and the $A7$ to *sc* transition pressure by performing variable-cell relaxation calculations for various target pressures. Then, for selected pressures below and above the transition, we calculate the electronic structure, phonon modes, and e-p coupling. These quantities are then used to study the pressure dependence of T_c.

A. Electron-phonon coupling formalism

We study the e-p coupling within a many-body formalism.[30–32] The e-p matrix element for the scattering of an electron in band n at wavevector $\mathbf{k}$ to a state in band m with wavevector $\mathbf{k}+\mathbf{q}$ by a phonon with mode index ν at wavevector $\mathbf{q}$ is given by

$$g^{\nu}_{mn}(\mathbf{k},\mathbf{q}) = \left(\frac{\hbar}{2M\omega_{\mathbf{q}\nu}}\right)^{1/2} \langle m,\mathbf{k}+\mathbf{q}|\delta_{\mathbf{q}\nu}V_{SCF}|n,\mathbf{k}\rangle. \quad (1)$$

In this expression, $|n,\mathbf{k}\rangle$ is the bare electronic Bloch state, $\omega_{\mathbf{q}\nu}$ is the screened phonon frequency, M is the ionic mass, and $\delta_{\mathbf{q}\nu}V_{SCF}$ is the derivative of the self-consistent potential with respect to a collective ionic displacement corresponding to phonon wavevector $\mathbf{q}$ and mode ν. The quantities entering into Eq. (1) are obtained from first-principles band structure and phonon calculations, as described in Sec. III B.

The main quantities to be calculated are the phonon linewidth $\gamma_{\mathbf{q}\nu}$, the phonon-mode-dependent coupling constant $\lambda_{\mathbf{q}\nu}$, the Eliashberg spectral function $\alpha^2F(\omega)$, and the average e-p coupling constant (or mass enhancement parameter) λ. In the Migdal approximation,[33] the phonon linewidth is given by

$$\gamma_{\mathbf{q}\nu} = \pi\omega_{\mathbf{q}\nu}\sum_{mn}\sum_{\mathbf{k}} w_{\mathbf{k}}\left|g^{\nu}_{mn}(\mathbf{k},\mathbf{q})\right|^2 \delta(\epsilon_{m,\mathbf{k}+\mathbf{q}}-\epsilon_F)\delta(\epsilon_{n,\mathbf{k}}-\epsilon_F), \quad (2)$$

where $w_{\mathbf{k}}$ is the k-point weight (normalized such that $\sum_{\mathbf{k}} w_{\mathbf{k}} = 2$). The sum over electron wavevectors $\mathbf{k}$ can be performed on a uniform grid over the whole BZ, or over the irreducible BZ (IBZ), with appropriate weights. The phonon-mode-dependent coupling constant is given by

$$\lambda_{\mathbf{q}\nu} = \frac{\gamma_{\mathbf{q}\nu}}{\pi N(\epsilon_F)\omega^2_{\mathbf{q}\nu}}. \quad (3)$$

In terms of the phonon linewidths, $\alpha^2F(\omega)$ can be written as[34]

$$\alpha^2F(\omega) = \frac{1}{2\pi N(\epsilon_F)}\sum_{\mathbf{q}\nu} w_{\mathbf{q}}\frac{\gamma_{\mathbf{q}\nu}}{\omega_{\mathbf{q}\nu}}\delta(\omega-\omega_{\mathbf{q}\nu}). \quad (4)$$

The sum over phonon wavevector $\mathbf{q}$ is performed either on a uniform grid over the whole BZ, or over the IBZ, with appropriate weights $w_{\mathbf{q}}$, where $\sum_{\mathbf{q}} w_{\mathbf{q}} = 1$. In Eqs. (3) and (4), $N(\epsilon_F)$ is the density of states at ϵ_F per unit cell and per spin. The coupling constant λ is given by the integral

$$\lambda = 2\int_0^{\infty}\frac{\alpha^2F(\omega)}{\omega}d\omega. \quad (5)$$

Other important frequency moments of $\alpha^2F(\omega)$ are defined as follows:

$$\langle\omega^2\rangle = \frac{2}{\lambda}\int_0^{\infty}\omega\alpha^2F(\omega)d\omega \quad (6)$$

and

$$\omega_{\log} = \exp\left[\frac{2}{\lambda}\int_0^{\infty}\log\omega\frac{\alpha^2F(\omega)}{\omega}d\omega\right]. \quad (7)$$

Conventional electron-phonon superconductors are well described by the Eliashberg theory of superconductivity,[35] which is based on the BCS theory.[36] Within the isotropic approximation to the Eliashberg theory, we can determine the superconducting transition temperature T_c using the Allen-Dynes-modified McMillan equation:[37,38]

$$T_c = \frac{\omega_{\log}}{1.2}\exp\left[-\frac{1.04(1+\lambda)}{\lambda-\mu^*(1+0.62\lambda)}\right], \quad (8)$$

where μ^* is the Coulomb psuedopotential.[39]

B. Computational details

All of our electronic structure, phonon, and e-p calculations are performed from first-principles using the QUANTUM-ESPRESSO code[40] (QE) within the framework of density-functional theory[41,42] and with the local-density approximation (LDA).[43,44] The As ions are modeled using norm-conserving pseudopotentials,[45] while the valence electron states (five valence electrons per atom) are calculated using a plane-wave basis set[46] with an energy cutoff of 50 Ry.

Following previous studies,[24,26–28] we calculate the structure of As as a function of pressure by performing a variable-cell relaxation at constant pressure until the components of the forces on the atoms are less than 10^{-4} Ry/a.u. and the pressure is within 0.05 GPa of the target pressure. For all such relaxations, the starting structure is that of the experimental $A7$ structure[21] (see Sec. II).

Close to the transition pressure, the structure is sensitive to the k-point sampling of the BZ and the smearing used to occupy the electronic states. We found that using a Methfessel-Paxton (MP) smearing[47] of 0.3 eV and a $40\times40\times40$ shifted k-grid[48] allowed us to converge a_{rhom}, α, and u to within 0.01 Å, 0.1°, and 0.001, respectively, for the pressures we considered. These parameters are comparable to those used in Ref. 28, in which convergence was studied in detail.

For selected pressures, we calculate the electronic structure, phonons, and e-p coupling. Convergence of $\gamma_{\mathbf{q}\nu}$ and $\alpha^2F(\omega)$

[Eqs. (2) and (4)] requires the calculation of e-p matrix elements on a fine grid for both electrons and phonons. With the electron-phonon-Wannier method,[18,19] such a calculation can be performed with relatively low computational cost. The e-p matrix elements are computed from first principles on coarse electron and phonon grids and then interpolated onto arbitrarily fine k- and q-grids by Wannier-Fourier interpolation. The accuracy of this interpolation is checked by examining the real space localization of the electronic Wannier states and the phonon perturbation (related to the range of the interatomic force constants). Maximally localized Wannier functions[49,50] are obtained with the WANNIER90 code.[51]

The computational parameters for the e-p calculations are as follows. For pressures below the structural transition, we use the unit cell of the $A7$ structure. The self-consistent charge density is computed using a $20 \times 20 \times 20$ shifted k-grid and a 0.3 eV MP smearing for the occupation of the electronic states. Wannier functions are computed for the lowest eight bands, including all bands crossing ϵ_F. For the e-p matrix elements, electronic states are computed on a uniform $6 \times 6 \times 6$ Γ-centered coarse k-grid, while phonons are computed using a $6 \times 6 \times 6$ Γ-centered coarse q-grid. The matrix elements are interpolated onto uniform Γ-centered fine k- and q-grids of $80 \times 80 \times 80$ and $14 \times 14 \times 14$, respectively.

For pressures above the structural transition, we use the unit cell for the sc structure. The density is computed using a $32 \times 32 \times 32$ shifted k-grid with a 0.3 eV MP smearing for the occupations. Wannier functions are computed for the lowest four bands. Grids centered at Γ of $6 \times 6 \times 6$ (coarse) and $100 \times 100 \times 100$ (fine) for electrons and $6 \times 6 \times 6$ (coarse) and $16 \times 16 \times 16$ (fine) for phonons were used. In Eq. (2), the δ functions are approximated by Gaussian functions of width 0.01 Ry for all pressures.

The phonon calculations are performed using density-functional perturbation theory (DFPT),[52] as implemented in QE. No anharmonic contribution is included. Near the structural phase transition, the $A7$ Γ_1 optical and sc R phonon modes soften considerably, and the anharmonic contributions are significant.[9,14] Since the pressures at which we perform our e-p calculations are not too close to the transition, the harmonic approximation is satisfactory: Although there is some error in the phonon frequencies for these particular modes, it does not effect the main results. Anharmonic effects are discussed further in Sec. IV.

IV. RESULTS

A. Determination of As structure as a function of pressure

We performed variable-cell relaxation calculations for target pressures at 5 GPa intervals in the range 0–50 GPa. The $A7$ lattice parameters, as well as the nearest neighbor (d_1) and next-nearest neighbor (d_2) distances between As atom positions, are plotted in Fig. 1. The lattice constants at 0 GPa agree well with previous LDA calculations.[8,10,22–24,28]

The $A7$ and sc structures are most easily distinguished by comparing d_1 and d_2 [Fig. 1(d)]. When $d_1 \neq d_2$, the crystal is in the $A7$ structure, while $d_1 = d_2$ is in the sc structure. Our calculated transition pressure is between 20 and 25 GPa, consistent with the most detailed previous theoretical work.[28]

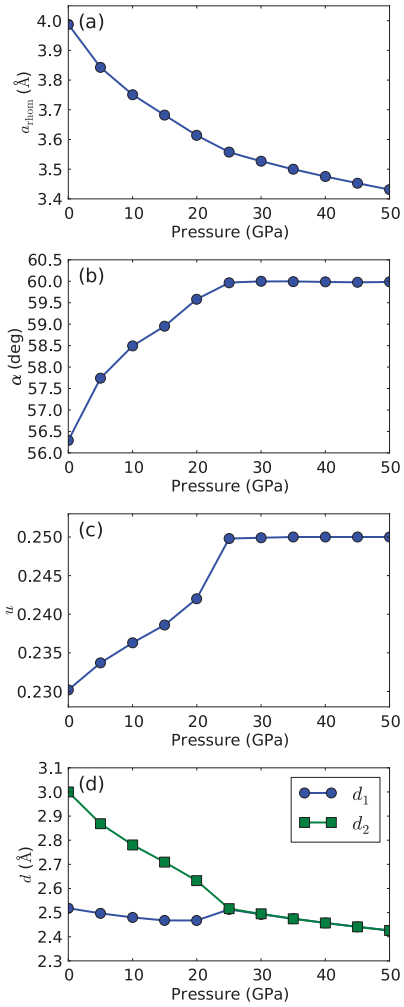

FIG. 1. (Color online) Lattice parameters (a) $a_{\rm rhom}$, (b) α, and (c) u, and (d) nearest neighbor d_1 and next-nearest neighbor d_2 distances for variable-cell relaxation calculations of As in the $A7$ structure with target pressures between 0 and 50 GPa. The transition pressure from $A7$ to sc is found to be between 20 and 25 GPa.

A fit of the calculated energy versus volume values from 0 to 50 GPa to a Murnaghan equation of state[53] (EOS) gives $B_0 = 57.2$ GPa and $B' = 4.21$ for the bulk modulus and its derivative, respectively, in reasonable agreement with the experimental values of 55.6 GPa and 4.4 (Ref. 5) and 58.4 GPa and 3.34 (Ref. 6). It is known that, compared to experiment, the LDA tends to underestimate the volume at a given pressure. To convert our calculated pressure to an experimental one, we input the calculated volume into a Murnaghan EOS with experimental B_0 and B' and use the resulting pressure. With this conversion procedure, the theoretical pressures of 20 and 25 GPa correspond to experimental pressures of 28 and 35 GPa, respectively, using parameters from Ref. 5, and 25 and 30 GPa, respectively, using parameters from Ref. 6. The respective experimental transition pressures of 32 and 25 GPa from the two experiments are consistent with our calculations, although the pressure resolution in our calculation is not very fine, and the method of relating calculated to experimental pressures is not rigorously justified. We study the electronic structure, phonons, and e-p coupling at three (theoretical) pressures

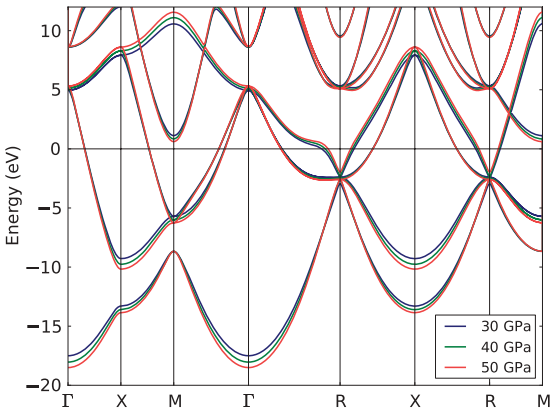

FIG. 2. (Color online) Electronic band structure for *sc* As at 30, 40, and 50 GPa. Energies are relative to ϵ_F.

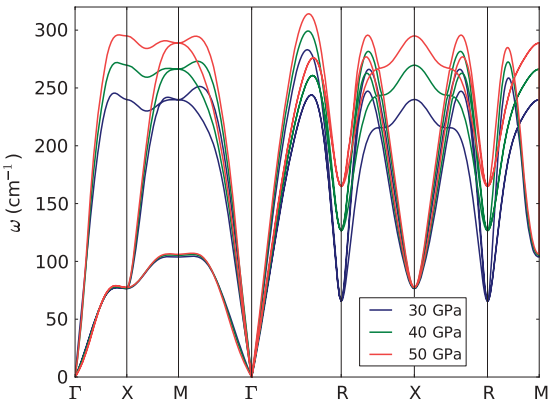

FIG. 4. (Color online) Phonon dispersion for *sc* As at 30, 40, and 50 GPa.

(0, 10, and 20 GPa) for which As is in the $A7$ structure below the transition, and three pressures (30, 40, and 50 GPa) for which As is in the *sc* structure above the transition.

B. As in the *sc* structure

Before discussing properties of As in the more complicated $A7$ structure, we present our results for *sc* As. The band structure along high-symmetry directions and the density of states $N(\epsilon)$ for *sc* As at 30, 40, and 50 GPa are given in Figs. 2 and 3. (Here we have normalized $N(\epsilon)$ to be per atom, with contributions from both spins summed.) At all pressures, three bands cross ϵ_F. The bands broaden but otherwise do not change significantly as pressure is increased. The most significant change in the electronic structure is the decrease in $N(\epsilon_F)$ as pressure is increased (Fig. 3). This trend is in agreement with the calculations of Ref. 14, although there are quantitative differences. Values for $N(\epsilon_F)$ are presented in Table I.

Figure 4 shows the phonon dispersions for *sc* As at 30, 40, and 50 GPa. Overall, as pressure increases, the phonon frequencies increase, as expected. A significant change in phonon frequency occurs for wavevectors near the R point in the BZ. Approaching the transition pressure from above, the R phonon softens significantly. Previous studies have indicated that Fermi surface nesting plays an important role in this phonon softening.[10,11]

The frequency of the R mode has been computed previously using the frozen phonon method.[9,14] In comparison to our calculations, the frequencies from Ref. 9 are softer at corresponding volumes. This discrepancy may be due to differences in k-point sampling or plane-wave energy cutoff. Our calculated frequencies are lower than those of Ref. 14 by approximately 50% at 30 GPa and 25% at 50 GPa. This difference indicates the degree of anharmonicity of the R mode, since anharmonic effects were included in Ref. 14 but not in the present study.

The e-p coupling parameter $\lambda_{\mathbf{q}} = \sum_\nu \lambda_{\mathbf{q}\nu}$ is plotted along high-symmetry directions in the BZ in Fig. 5. The coupling at R, reaching values of 35, 9.8, and 6.1 for 30, 40, and 50 GPa, respectively, is much larger than at other points in the BZ. The change in $\lambda_{\mathbf{q}}$ at R with pressure can mainly be attributed to the change in $\omega_{\mathbf{q}\nu}$, as the change in $\gamma_{\mathbf{q}\nu}$ is small, and the change in $N(\epsilon_F)$ is modest.

The calculated $F(\omega)$ and $\alpha^2F(\omega)$ for *sc* As are plotted in Fig. 6 (a Gaussian smearing of width 0.5 meV ≈ 4 cm^{-1} is used). The shape of $\alpha^2F(\omega)$ is very similar to that of $F(\omega)$. The

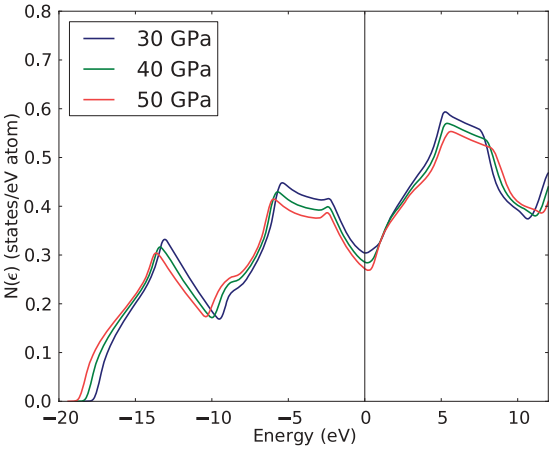

FIG. 3. (Color online) Electronic density of states $N(\epsilon)$ for *sc* As at 30, 40, and 50 GPa. Energies are relative to ϵ_F.

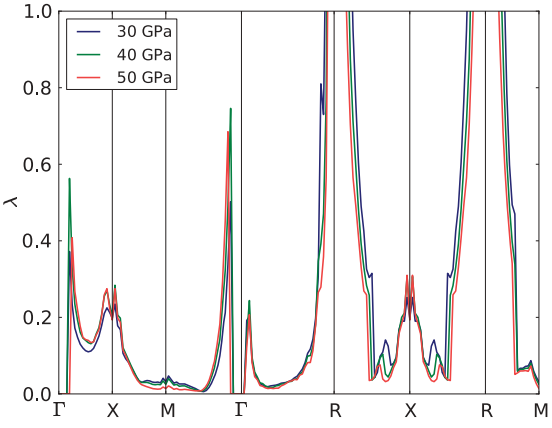

FIG. 5. (Color online) Electron-phonon coupling parameter $\lambda_{\mathbf{q}}$ for *sc* As at 30, 40, and 50 GPa. The values of the peak at R are 35, 9.8, and 6.1 for 30, 40, and 50 GPa, respectively.

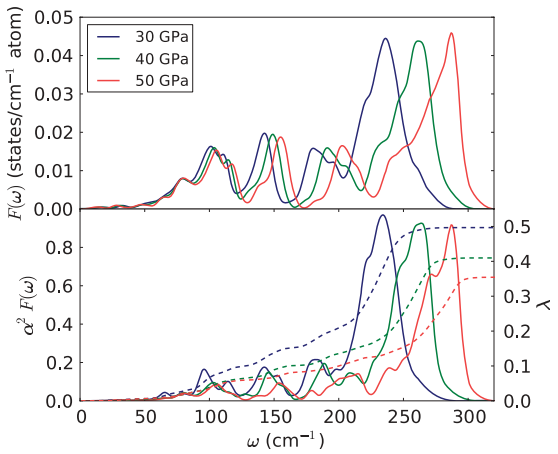

FIG. 6. (Color online) Phonon density of states $F(\omega)$ (top), Eliashberg spectral function $\alpha^2F(\omega)$ (bottom, solid), and integrated λ (bottom, dashed) for sc As at 30, 40, and 50 GPa.

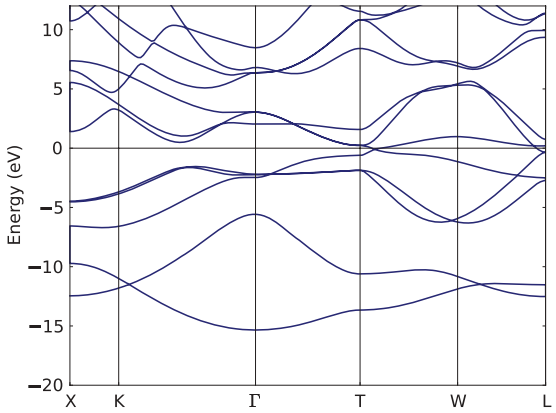

FIG. 7. (Color online) Electronic band structure for $A7$ As at 0 GPa. Energies are relative to ϵ_F.

main difference is the enhanced weight for higher frequencies for $\alpha^2F(\omega)$ compared to $F(\omega)$.

The enhanced coupling to higher frequencies can be explained qualitatively as follows. Higher frequency modes correspond to compression or stretching of bonds, while lower frequency modes correspond to bond bending. Modes which change bond length modify the overlap of the half-filled p-like orbitals and thus change the electronic structure near ϵ_F, in a manner similar to a Peierls distortion. Such modes therefore couple strongly to electrons at ϵ_F. On the other hand, bond-bending modes do not affect the overlap of p-like orbitals as much, and therefore couple less strongly.

The integrated λ as a function of frequency is also plotted in Fig. 6 (bottom) for the three pressures considered. As $\alpha^2F(\omega)$ shifts to higher frequencies with higher pressure, λ decreases.

The calculated $\omega_{\log}$, $\langle\omega^2\rangle^{1/2}$, λ, and T_c (for two values of μ^*) are given in Table I. For sc As, as pressure increases, the average phonon frequency increases, $N(\epsilon_F)$ decreases, and λ decreases, leading to a decrease in T_c. Similar values for $N(\epsilon_F)$ and λ were obtained in a previous study,[54] although those calculations were not from first principles.

As pressure is decreased towards the transition from above, the increase in coupling $\lambda_{\mathbf{q}}$ is much greater at points near R than at other regions of the BZ. As noted previously, this increase in coupling is mainly due to phonon softening. An interesting question is how much this particular coupling to phonons near R directly contributes to the increase in total λ. To answer this question, we estimate what the increase in λ from 50 to 30 GPa would be if there were no special coupling enhancement near R. We calculate λ^P_{cut}, the coupling at pressure P due to all q-points at least $0.3(\pi/a_{\text{cubic}})$ away from R in reciprocal space, where a_{cubic} is the sc lattice constant. We then get a new value $\lambda_{\text{scaled}} = \lambda^{50\text{GPa}}(\lambda^{30\text{GPa}}_{\text{cut}}/\lambda^{50\text{GPa}}_{\text{cut}})$, which is the estimated coupling at 30 GPa without the special coupling enhancement at R. We find $\lambda_{\text{scaled}} = 0.46$, while $\lambda^{30\text{GPa}} = 0.50$. Therefore, the extra coupling near R contributes a 0.04 increase in λ, whereas the overall increase in λ going from 50 to 30 GPa is 0.14. We conclude that the increase in total λ is not dominated by the R mode; rather, a broad range of modes contributes to the increase. The overall trends in e-p parameters as a function of pressure will be discussed further in Sec. V.

C. As in the $A7$ structure

The calculated band structure (Fig. 7) and $N(\epsilon)$ (Fig. 8) at 0 GPa are in good agreement with previous theoretical studies.[8,10,25] As pressure increases to 20 GPa, the bands broaden and $N(\epsilon_F)$ increases significantly, as seen in the plot of $N(\epsilon)$ (Fig. 8). Values for $N(\epsilon_F)$ are given in Table I. A similar increase in $N(\epsilon_F)$ was found in Ref. 14, although there are quantitative differences. Note also how the shape of $N(\epsilon)$ for $A7$ As approaches that of sc As (Fig. 3) as the pressure increases towards the structural transition pressure.

The phonon dispersions at 0, 10, and 20 GPa are given in Fig. 9. An overall hardening of phonons occurs with increased pressure. However, the optical phonon modes at Γ soften with increased pressure as the structural transition

TABLE I. Calculated frequency moments, $N(\epsilon_F)$, electron-phonon coupling parameter λ, and superconducting transition temperature T_c for As at various pressures.

P (GPa)	Structure	$\omega_{\log}$ (K)	$\langle\omega^2\rangle^{1/2}$ (K)	$N(\epsilon_F)$ (states/eV atom)	λ	T_c (K) $\mu^* = 0.10$	T_c (K) $\mu^* = 0.15$
0	$A7$	158	199	0.073	0.19	0.00	0.00
10	$A7$	194	232	0.148	0.32	0.19	0.01
20	$A7$	227	260	0.247	0.43	1.34	0.35
30	sc	253	284	0.290	0.50	2.99	1.19
40	sc	283	317	0.266	0.41	1.36	0.32
50	sc	298	341	0.253	0.35	0.58	0.07

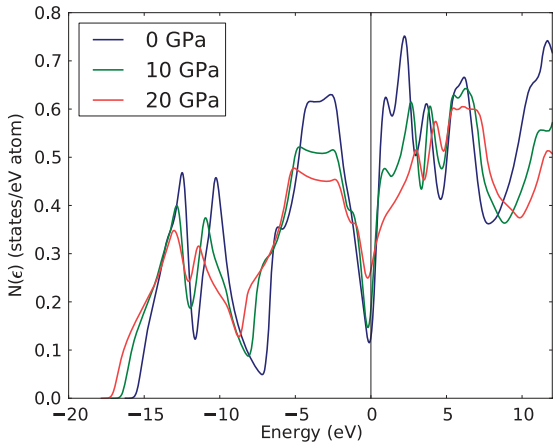

FIG. 8. (Color online) Electronic density of states $N(\epsilon)$ for $A7$ As at 0, 10, and 20 GPa. Energies are relative to ϵ_F.

is approached. As pressure is increased and the structure moves closer to sc, the splitting between the optical modes at Γ decreases. These modes become degenerate when the sc structure is reached. The dispersion for 0 GPa is consistent with previous experimental[55] and theoretical[11] studies. Slight differences are likely due to the slightly smaller volume used for the present calculation. For all pressures considered, the calculated Γ_1 optical frequencies are in good agreement with previous frozen phonon calculations.[8,14] The calculations, which include only the harmonic contribution, underestimate the experimental Raman frequencies,[6] with increasing error as the transition pressure is approached, indicating the increasing anharmonicity of this phonon mode.

Figure 10 (top) shows $F(\omega)$ for 0, 10, and 20 GPa. Separate contributions from the acoustic and optical branches are shown, as well as the total. In general, both branches shift towards higher frequencies with higher pressure; the acoustic branch broadens in frequency, while the width of the optical branch does not change much. A low frequency tail, corresponding to the optical modes near Γ, appears in $F(\omega)$ for higher pressures.

The total and separate acoustic and optical contributions to $\alpha^2F(\omega)$ are shown in Fig. 10 (bottom). The higher frequency optical modes have a greater e-p coupling than the lower frequency acoustic modes, as seen by comparing the spectral weight of $F(\omega)$ and $\alpha^2F(\omega)$. A similar effect for sc As was noted and explained qualitatively in Sec. IV B.

The integrated λ is also shown in Fig. 10 (bottom). The total λ increases significantly, from 0.19 to 0.43, when pressure is increased from 0 GPa to 20 GPa. In the acoustic modes, a significant increase of ∼0.1 in the integrated λ occurs when going from 0 to 10 GPa, while a further increase to 20 GPa does not increase the contribution from acoustic modes to λ much. The optical mode contribution increases more than the acoustic mode contribution upon increase of pressure from 10 to 20 GPa.

The coupling of the optical modes at Γ is very large, with $\lambda_{\mathbf{q}}$ reaching a value of 20 at 20 GPa. Both an increasing e-p matrix element and phonon softening contribute to this large value of $\lambda_{\mathbf{q}}$. However, the phase space near Γ is small, as seen in Fig. 10 (top right), where in the range 100–200 cm^{-1}, the optical contribution to $F(\omega)$ is small. Therefore, although the coupling is large for the optical modes at Γ, the contribution of these modes to the increase in total λ with increasing pressure is quite modest. From the integrated λ curve, we estimate that the contribution of these modes to the increase in λ from 0 to 20 GPa is about 0.05, while the total increase in λ is 0.24. Furthermore, if anharmonic effects were included in the calculation, the e-p coupling of the optical modes near Γ would likely decrease due to an increased phonon frequency, leading to an even smaller contribution to the increase in total λ. Thus the phonon softening itself is not the main direct cause of the increase in λ with increasing pressure.

The primary importance of the phonon softening is indirect. Phonon softening leads to structural changes and changes in electronic structure, the most important of which is the increase in $N(\epsilon_F)$. As discussed in Sec. V, the increase in $N(\epsilon_F)$ is the dominant cause of increasing λ with pressure in the $A7$ structure. The e-p quantities for $A7$ As are summarized in Table I.

V. DISCUSSION

To understand the relative contributions of changes in phonon frequencies, $N(\epsilon_F)$, and e-p matrix elements to changes in λ as a function of pressure, we consider the relation[37]

$$\lambda = \frac{N(\epsilon_F)\langle g^2\rangle}{M\langle\omega^2\rangle}, \tag{9}$$

where $\langle g^2\rangle$ is the average over the Fermi surface of the e-p matrix element, and M is the ionic mass. Values for $\langle g^2\rangle$ are

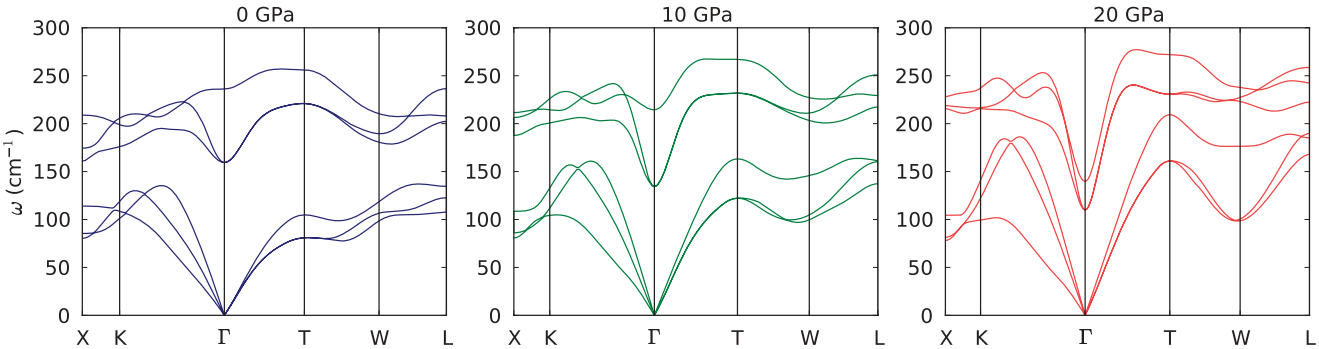

FIG. 9. (Color online) Phonon dispersion $\omega_{\mathbf{q}\nu}$ for $A7$ As at 0 GPa (left), 10 GPa (middle), and 20 GPa (right).

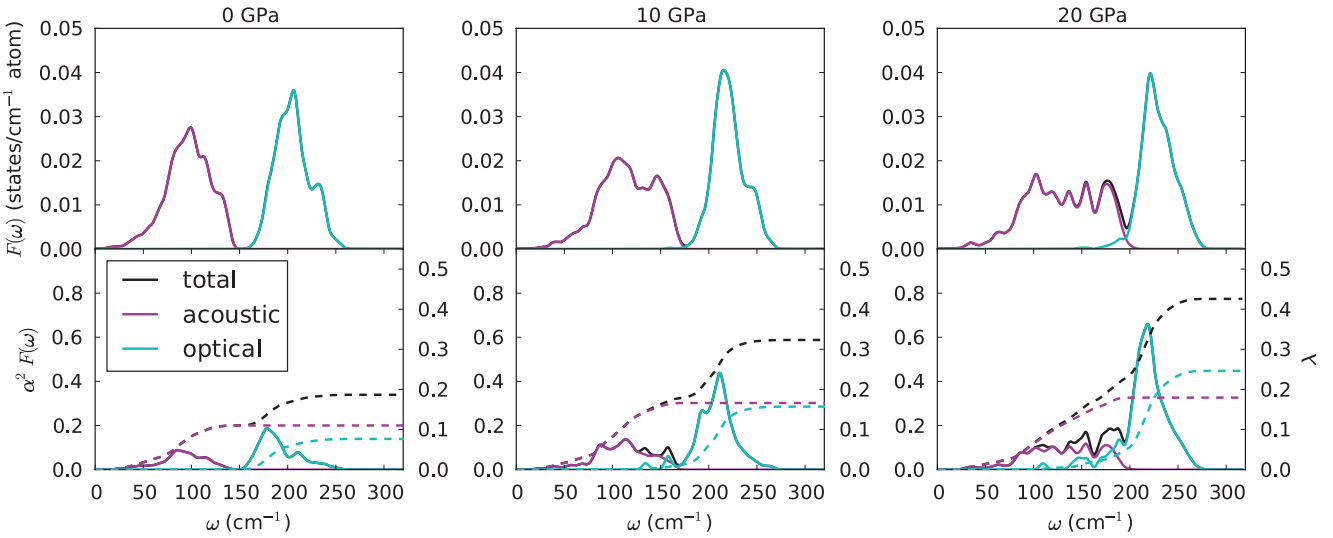

FIG. 10. (Color online) Total, acoustic, and optical contributions to the phonon density of states $F(\omega)$ (top), Eliashberg spectral function $\alpha^2 F(\omega)$ (bottom, solid), and integrated λ (bottom, dashed) for $A7$ As at 0 GPa (left), 10 GPa (middle), and 20 GPa (right).

obtained indirectly using Eq. (9) from the calculated values of λ, $N(\epsilon_F)$, and $\langle\omega^2\rangle$, as given in Table I. (Other general relations between quantities relevant for superconductivity are presented in Ref. 56.)

To analyze relative changes as a function of pressure, we take the natural logarithm of the quantities, normalized to the value at 0 GPa, and plot them in Fig. 11 for the range 10–50 GPa. From Eq. (9), we have

$$\log\frac{\lambda}{\lambda_0} = \log\frac{N(\epsilon_F)}{N(\epsilon_F)_0} + \log\frac{\langle g^2\rangle}{\langle g^2\rangle_0} + \log\frac{\langle\omega^2\rangle_0}{\langle\omega^2\rangle}, \qquad (10)$$

where the subscript 0 denotes the value at 0 GPa. Positive values of $\log(x/x_0)$ indicate an increase in the value of x as compared to the value at 0 GPa, while negative values indicate a decrease. Note also that for the McMillan-Hopfield parameter $\eta = N(\epsilon_F)\langle g^2\rangle$, we have $\log(\eta/\eta_0) = \log(N(\epsilon_F)/N(\epsilon_F)_0) + \log(\langle g^2\rangle/\langle g^2\rangle_0)$, so that in Fig. 11 the sum of the contributions from $N(\epsilon_F)$ and $\langle g^2\rangle$ equals the contribution from η. As discussed in Ref. 37, η can be

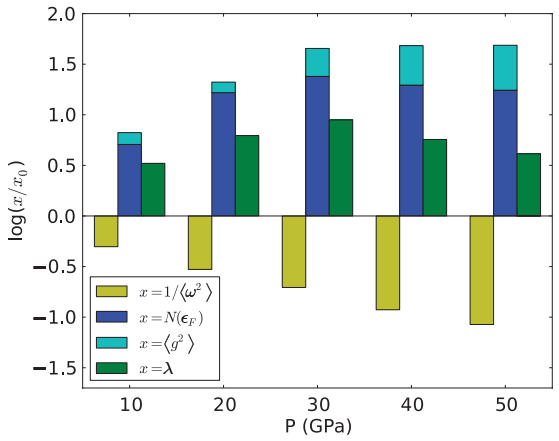

FIG. 11. (Color online) Trends in average phonon frequency $\langle\omega^2\rangle$, $N(\epsilon_F)$, average e-p matrix element $\langle g^2\rangle$, and e-p coupling λ as a function of pressure. The subscript 0 denotes the value at 0 GPa.

considered as an electronic contribution to λ and $\langle\omega^2\rangle$ a phononic contribution.

Figure 11 shows the following effects as pressure is increased. The increase in phonon frequencies acts in the direction of lowering λ. The average matrix elements $\langle g^2\rangle$ generally increase, but the effect is not as significant as the effects from $N(\epsilon_F)$ and phonon frequencies. For $A7$ As, the dominant cause of the increase in λ is the large increase in $N(\epsilon_F)$, which overcomes the increase in $\langle\omega^2\rangle$. For sc As, it is interesting that the decrease in $N(\epsilon_F)$ with increasing pressure is compensated by the increase in $\langle g^2\rangle$, so that η is almost constant as a function of pressure. Equivalently, λ is almost proportional to $1/\langle\omega^2\rangle$; i.e., the dominant effect in the decrease of λ with increasing pressure is the increase in phonon frequency. The overall trend for λ is to increase with pressure in the $A7$ structure, and decrease with pressure in the sc structure.

In Fig. 12, we compare our calculations for T_c as a function of pressure to experimental results from Chen *et al.*[14] The calculated values are shifted to the experimental pressures, following the procedure described in Sec. IV A. For calculations 1A and 2A, we use the EOS parameters from Kikegawa and Iwasaki[5] and Beister *et al.*,[6] respectively. For each set of points, one point (with calculated pressure 30 GPa) lies within the pressure range for which a finite T_c was experimentally measured by Chen *et al.* Using the McMillan equation, we adjust μ^* to match the calculated T_c to the experimental value at this pressure. Within each set of points, the same μ^* is used for the other pressures. We obtain $\mu^* = 0.128$ and 0.117 for calculations 1A and 2A, respectively.

The validity of our results is supported by the fact that these values for μ^* are close to the accepted values for other conventional superconductors.[37,38] In addition, we find that at pressures below and above the peak in T_c, the calculated T_c is below 1.7 K; this result is consistent with the experiment. However, we note that a transition from sc to another structure was observed experimentally at around 48 GPa (Ref. 57) and is not accounted for in the present calculation.

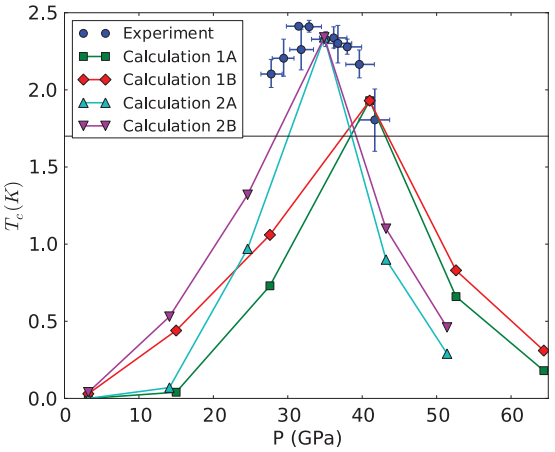

FIG. 12. (Color online) Superconducting transition temperature T_c as a function of pressure. Blue circles denote experimental results, with error bars, from Ref. 14. For the calculated values, the pressure is determined from the experimental Murnaghan equation of state (EOS) parameters, using the calculated volume as input. For Calculations 1A (green squares) and 1B (red diamonds), $\mu^* = 0.128$ at 41 GPa, and the EOS parameters are from Ref. 5. For Calculation 2A (cyan up-triangles) and 2B (magenta down-triangles), $\mu^* = 0.117$ at 35 GPa, and the EOS parameters are from Ref. 6. For Calculations 1A and 2A, μ^* is constant for all pressures, while for Calculations 1B and 2B, μ^* varies with pressure according to Eq. (11) in the text. The horizontal line at 1.7 K denotes the lower limit of accessible temperatures in the experiment.

We also consider how μ^* might change with pressure. We expect μ^* to vary with $N(\epsilon_F)$ as the pressure changes; a reasonable relation is given by a modified Bennemann-Garland formula:[58–60]

$$\mu^* = \frac{CN(\epsilon_F)}{1 + N(\epsilon_F)}, \tag{11}$$

where C is a constant and $N(\epsilon_F)$ is given in states/eV atom. The effect on T_c is shown in Fig. 12. Calculations 1B and 2B are the same as 1A and 2A, respectively, except that μ^* is varied with pressure according to Eq. (11), using the calculated $N(\epsilon_F)$ values (Table I). For calculation 1B (2B), we set $C = 0.57$ (0.52) so that the μ^* of 0.128 (0.117) matches calculation 1A (2A) at the point with a theoretical pressure of 30 GPa. If this variation in μ^* with pressure is included, the peak in T_c is somewhat broader than if μ^* is taken to be constant, but the results remain consistent with experiment. While the changes with pressure of μ^* and λ have opposite effects on T_c, the changes in λ dominate.

VI. CONCLUSION

Our first-principles e-p coupling calculations for As at pressures above and below the $A7$ to sc transition show that the peak in T_c is indeed related to the structural transition, as suggested by previous studies. The main factor in the increase in λ and hence T_c with increasing pressure below the transition is the large increase in $N(\epsilon_F)$, while the decrease in λ above the transition is mainly due to the increase in average phonon frequency as pressure increases. The softening and large e-p coupling of the $A7$ Γ_1 optical and sc R modes as the transition is approached do not make a large direct contribution to the increase in λ; nevertheless, they play important roles in the peak in T_c because they drive the structural transition. The physical mechanisms discussed here have relevance for e-p coupling in other Group V elements as well.[61]

ACKNOWLEDGMENTS

This work was supported by National Science Foundation Grant No. DMR10-1006184 and by the Director, Office of Science, Office of Basic Energy Sciences, Materials Sciences and Engineering Division, US Department of Energy under Contract No. DE-AC02-05CH11231. Computational resources have been provided by DOE at Lawrence Berkeley National Laboratory's NERSC facility and the Lawrencium computational cluster resource provided by the IT Division at the Lawrence Berkeley National Laboratory.

*kchan@civet.berkeley.edu

[1] C. Buzea and K. Robbie, Supercond. Sci. Technol. **18**, R1 (2005).
[2] K. Shimizu, H. Ishikawa, D. Takao, T. Yagi, and K. Amaya, Nature (London) **419**, 597 (2002).
[3] V. V. Struzhkin, M. I. Eremets, W. Gan, H.-k. Mao, and R. J. Hemley, Science **298**, 1213 (2002).
[4] S. Deemyad and J. S. Schilling, Phys. Rev. Lett. **91**, 167001 (2003).
[5] T. Kikegawa and H. Iwasaki, J. Phys. Soc. Jpn. **56**, 3417 (1987).
[6] H. J. Beister, K. Strössner, and K. Syassen, Phys. Rev. B **41**, 5535 (1990).
[7] M. H. Cohen, L. M. Falicov, and S. Golin, IBM J. Res. Dev. **8**, 215 (1964).
[8] R. J. Needs, R. M. Martin, and O. H. Nielsen, Phys. Rev. B **33**, 3778 (1986).
[9] K. J. Chang and M. L. Cohen, Phys. Rev. B **33**, 7371 (1986).
[10] L. F. Mattheiss, D. R. Hamann, and W. Weber, Phys. Rev. B **34**, 2190 (1986).
[11] S. Shang, Y. Wang, H. Zhang, and Z.-K. Liu, Phys. Rev. B **76**, 052301 (2007).
[12] I. V. Berman and N. B. Brandt, Pis'ma Zh. Eksp Teor. Fiz. **10**, 88 (1969).
[13] H. Kawamura and J. Wittig, Physica B + C **135**, 239 (1985).
[14] A. L. Chen, S. P. Lewis, Z. Su, P. Y. Yu, and M. L. Cohen, Phys. Rev. B **46**, 5523 (1992).
[15] D. Kasinathan, J. Kuneš, A. Lazicki, H. Rosner, C. S. Yoo, R. T. Scalettar, and W. E. Pickett, Phys. Rev. Lett. **96**, 047004 (2006).
[16] T. Bazhirov, J. Noffsinger, and M. L. Cohen, Phys. Rev. B **82**, 184509 (2010).
[17] T. Bazhirov, J. Noffsinger, and M. L. Cohen, Phys. Rev. B **84**, 125122 (2011).
[18] F. Giustino, M. L. Cohen, and S. G. Louie, Phys. Rev. B **76**, 165108 (2007).
[19] J. Noffsinger, F. Giustino, B. D. Malone, C.-H. Park, S. G. Louie, and M. L. Cohen, Comput. Phys. Commun. **181**, 2140 (2010).

[20]For a more detailed description of the *A*7 structure, see Ref. 8 or other references cited in this paper.
[21]D. Schiferl and C. S. Barrett, J. Appl. Crystallogr. **2**, 30 (1969).
[22]R. J. Needs, R. M. Martin, and O. H. Nielsen, Phys. Rev. B **35**, 9851 (1987).
[23]K. Seifert, J. Hafner, J. Furthmuller, and G. Kresse, J. Phys.: Condens. Matter **7**, 3683 (1995).
[24]C. R. da Silva and R. M. Wentzcovitch, Comput. Mater. Sci. **8**, 219 (1997).
[25]U. Häussermann, K. Söderberg, and R. Norrestam, J. Am. Chem. Soc. **124**, 15359 (2002).
[26]M. Durandurdu, Phys. Rev. B **72**, 073208 (2005).
[27]W. Feng, S. Cui, H. Hu, and H. Liu, Physica B: Condens. Matter **400**, 22 (2007).
[28]P. Silas, J. R. Yates, and P. D. Haynes, Phys. Rev. B **78**, 174101 (2008).
[29]E. S. Zijlstra, N. Huntemann, and M. E. Garcia, New J. Phys. **10**, 033010 (2008).
[30]J. R. Schrieffer, *Theory of Superconductivity* (Benjamin, New York, 1964).
[31]G. Grimvall, *The Electron-Phonon Interaction in Metals* (North-Holland, New York, 1981).
[32]P. B. Allen and B. Mitrović, in *Solid State Physics*, edited by F. S. Henry Ehrenreich and D. Turnbull, Vol. 37 of *Solid State Physics* (Academic Press, New York, 1983), pp. 1–92.
[33]A. B. Migdal, Zh. Eksp. Teor. Fiz. **34**, 1438 (1958).
[34]P. B. Allen, Phys. Rev. B **6**, 2577 (1972).
[35]G. M. Eliashberg, Zh. Eksp. Teor. Fiz. **38**, 966 (1960).
[36]J. Bardeen, L. N. Cooper, and J. R. Schrieffer, Phys. Rev. **108**, 1175 (1957).
[37]W. L. McMillan, Phys. Rev. **167**, 331 (1968).
[38]P. B. Allen and R. C. Dynes, Phys. Rev. B **12**, 905 (1975).
[39]P. Morel and P. W. Anderson, Phys. Rev. **125**, 1263 (1962).
[40]P. Giannozzi, S. Baroni, N. Bonini, M. Calandra, R. Car, C. Cavazzoni, D. Ceresoli, G. L. Chiarotti, M. Cococcioni, I. Dabo *et al*., J. Phys.: Condens. Matter **21**, 395502 (2009).
[41]P. Hohenberg and W. Kohn, Phys. Rev. **136**, B864 (1964).
[42]W. Kohn and L. J. Sham, Phys. Rev. **140**, A1133 (1965).
[43]D. M. Ceperley and B. J. Alder, Phys. Rev. Lett. **45**, 566 (1980).
[44]J. P. Perdew and A. Zunger, Phys. Rev. B **23**, 5048 (1981).
[45]G. B. Bachelet, D. R. Hamann, and M. Schlüter, Phys. Rev. B **26**, 4199 (1982).
[46]J. Ihm, A. Zunger, and M. L. Cohen, J. Phys. C **12**, 4409 (1979).
[47]M. Methfessel and A. T. Paxton, Phys. Rev. B **40**, 3616 (1989).
[48]H. J. Monkhorst and J. D. Pack, Phys. Rev. B **13**, 5188 (1976).
[49]N. Marzari and D. Vanderbilt, Phys. Rev. B **56**, 12847 (1997).
[50]I. Souza, N. Marzari, and D. Vanderbilt, Phys. Rev. B **65**, 035109 (2001).
[51]A. A. Mostofi, J. R. Yates, Y.-S. Lee, I. Souza, D. Vanderbilt, and N. Marzari, Comput. Phys. Commun. **178**, 685 (2008).
[52]S. Baroni, S. de Gironcoli, A. Dal Corso, and P. Giannozzi, Rev. Mod. Phys. **73**, 515 (2001).
[53]F. D. Murnaghan, Proceedings National Academy Sciences **30**, 244 (1944).
[54]B. Palanivel, M. Rajagopalan, and S. Natarajan, High Press. Res. **10**, 469 (1992).
[55]W. Reichardt and K. H. Rieder, in *Proceedings of the Conference on Neutron Scattering: Gatlinburg, Tennessee*, edited by R. M. Moon (Energy Research and Development Administration, Washington, DC, 1976), Vol. 1, p. 181.
[56]J. E. Moussa and M. L. Cohen, Phys. Rev. B **74**, 094520 (2006).
[57]R. G. Greene, H. Luo, and A. L. Ruoff, Phys. Rev. B **51**, 597 (1995).
[58]D. Papaconstantopoulos and B. Klein, Physica B + C **107**, 725 (1981).
[59]K. H. Bennemann and J. W. Garland, AIP Conf. Proc. **4**, 103 (1972).
[60]J. W. Garland and K. H. Bennemann, AIP Conf. Proc. **4**, 255 (1972).
[61]B. D. Malone, K. T. Chan, and M. L. Cohen (unpublished).